PHYSICAL REVIEW C **69**, 024305 (2004)

High-spin structure in ^{185}Os

T. Shizuma,[1] S. Mitarai,[2] G. Sletten,[3] R. A. Bark,[3] N. L. Gjørup,[3] H. J. Jensen,[3] M. Piiparinen,[3] J. Wrzesinski,[3] and Y. R. Shimizu[2]

[1]*Advanced Photon Research Center, Kansai Research Establishment, Japan Atomic Energy Research Institute, Tokai, Ibaraki, 319-1195, Japan*

[2]*Department of Physics, Kyushu University, Hakozaki, Fukuoka 812-8581, Japan*

[3]*Niels Bohr Institute, University of Copenhagen, DK-2100 Copenhagen, Denmark*

(Received 30 July 2003; published 23 February 2004)

High-spin states in ^{185}Os have been studied using the ^{176}Yb(^{13}C,$4n$) reaction at a beam energy of 65 MeV. Previously known one-quasiparticle bands have been extended to higher spins. New high-K bands based on three-quasiparticle excitation have been identified. Nilsson configurations are assigned based on the g factors deduced from $M1/E2$ branching ratios within the bands. In addition, a new isomer at 5007 keV has been found with a half-life of 18(2) ns. The hindrance in decays of the high-K intrinsic states are discussed in terms of the γ tunneling model where the low-K and high-K states interact through triaxial shape fluctuation.

DOI: 10.1103/PhysRevC.69.024305 PACS number(s): 21.10.Tg, 23.20.Lv, 27.70.+q

I. INTRODUCTION

In deformed nuclei with axially symmetric shapes, the projection of the total angular momentum on the nuclear symmetry axis $K(=\Sigma\Omega)$ is conserved. Consequently, transitions involving a K change greater than the transition multipole order, i.e., $\Delta K > \lambda$ are forbidden (*K selection rule*). In the region of nuclei of mass $A \approx 180$, both the proton and neutron Fermi surfaces lie among orbitals with large Ω. Therefore, high-K multiquasiparticle states can lie close to the yrast line [1]. According to the K selection rule, decays of high-K states take place in a stepwise fashion so as to minimize the K forbiddenness $\nu(=\Delta K - \lambda)$, and transitions with large ΔK are greatly retarded. However, transitions with low hindrances in spite of large K forbiddenness, which violate the K selection rule, were observed in ^{182}Os [2], ^{174}Hf [3], and ^{176}W [4]. So far, two mechanisms including Fermi-alignment Coriolis interaction [3,5–7] and shape fluctuation towards triaxial deformation [2,4,8,9] have been proposed for substantial K mixing between the low-K and high-K intrinsic states.

In this paper, we report on detailed high-spin structure in ^{185}Os based on new findings of excited levels including a $T_{1/2}=18$ ns isomer at 5007 keV. The decay rates of direct transitions from high-K to low-K states observed in ^{185}Os will be discussed in terms of the γ tunneling model.

II. EXPERIMENTS

High-spin states in ^{185}Os have been studied with the ^{176}Yb(^{13}C,$4n$) reaction at a beam energy of 65 MeV. A self-supported ^{176}Yb target enriched to 96.4% with a thickness of 2.0 mg/cm^2 was bombarded by a ^{13}C dc beam derived from the Niels Bohr Institute FN tandem accelerator. The target was thick enough to stop the recoiling residuals inside the target material so that delayed γ-ray transitions could be observed. In the reaction used, ^{184}Os ($5n$ exit channel)and ^{185}Os were chiefly produced.

Emitted γ rays were detected with the NORDBALL array consisting of twenty Compton-suppressed HP-Ge detectors and an inner ball of sixty BaF$_2$ detectors. In this array, four groups of five Ge detectors each are placed in rings at angles of 37°, 79°, 101°, and 143° with respect to the beam axis. The inner ball was used to measure the multiplicity and sum energy of the cascade γ rays. Events were recorded on magnetic tapes when two or more Ge detectors and at least one BaF$_2$ detector fired in coincidence. The time information of each γ-ray signal relative to a BaF$_2$ event was also measured. The coincidence time window was set to 200 ns so that half-lives less than ~100 ns could be reliably extracted. Approximately, 430×10^6 $\gamma\gamma$ and 30×10^6 $\gamma\gamma\gamma$ prompt events were collected. The prompt coincidences between any of Ge detectors were defined by an energy dependent time gate, which excludes events caused by neutrons and ensures no degradation of the detection efficiency of low-energy γ rays delayed due to their slower charge collection times in the Ge detectors. In addition, a time correlated event where the two γ rays are observed within 50–200 ns of each other was sorted into a two-dimensional matrix. This effectively distinguishes two types of γ-ray energy projection: (i) delayed projections, where gating on transitions that precede an isomer enables the projection of those events that follow the isomer; and (ii) the converse early projections. A level scheme of ^{185}Os was established using a combination of these coincident matrices with the aid of the computer code RADWARE [10]. The energy and efficiency calibrations of the Ge detectors were made by using ^{133}Ba, ^{134}Cs, and ^{152}Eu standard sources.

In order to determine multipole order (dipole or quadrupole) for transitions, DCO (directional angular correlation from oriented states) ratios can be used [11,12]. For the NORDBALL detector array, the DCO ratios are defined as

$$R_{\rm DCO}=\frac{I_\gamma \text{ at } 37° \text{ (or } 143°\text{)gated on } \gamma_{\rm G} \text{ at } 79° \text{ (or } 101°\text{)}}{I_\gamma \text{ at } 79° \text{ (or } 101°\text{)gated on } \gamma_{\rm G} \text{ at } 37° \text{ (or } 143°\text{)}}.$$

Since the angle of 101°(143°) is equivalent to that of 79°(37°) [12], the corresponding events can be summed

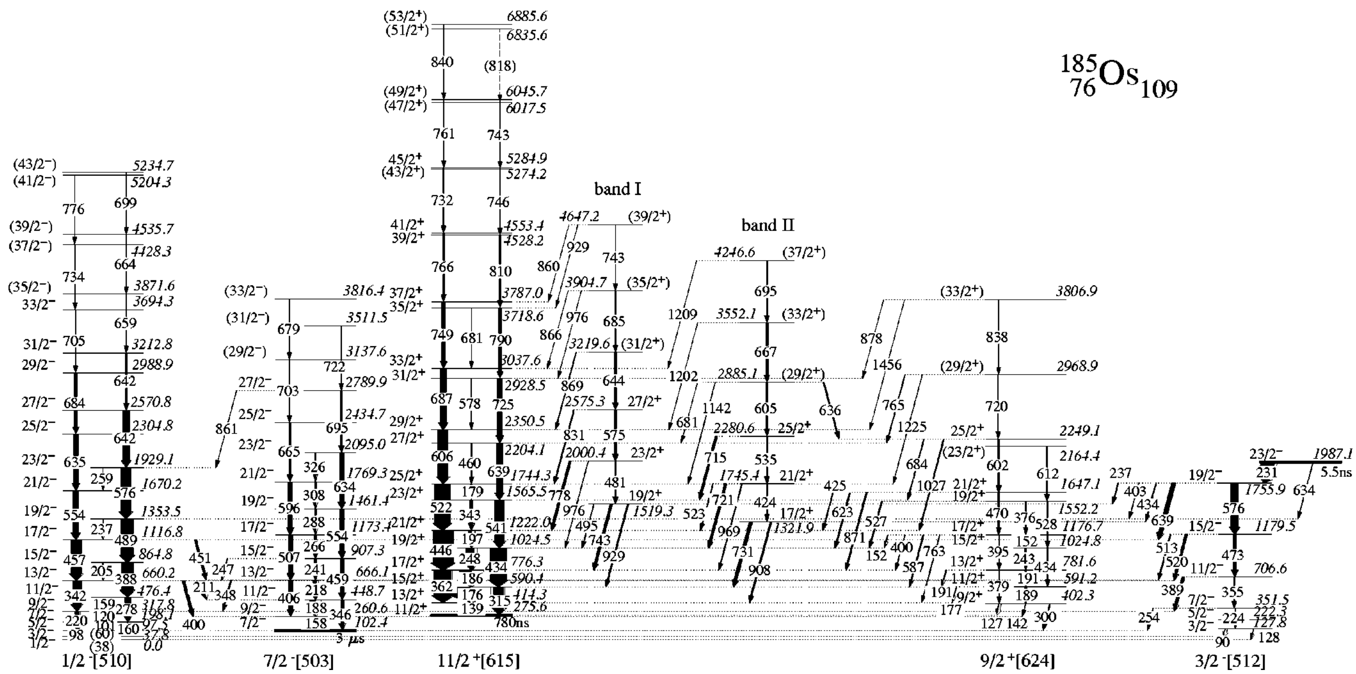

FIG. 1. Partial level scheme of ^{185}Os, showing the $1/2^-[510]$, $3/2^-[512]$, $7/2^-[503]$, $9/2^+[624]$, $11/2^+[615]$ bands and bands I and II. Decay paths for the $23/2^-$ isomer to the $1/2^-[510]$ (634 keV) and $3/2^-[512]$ (231 keV) bands are also illustrated. The width of the arrows is proportional to the γ-ray intensities (black) and the calculated intensities of electron conversion (white).

when the DCO matrices are created. In the DCO analysis, the stretched $\Delta I = 2$ transitions that are close to the γ ray of interest are generally used as the gate. In this case, the DCO ratio approaches 1 for stretched quadrupole ($\Delta I = 2$) and unstretched dipole ($\Delta I = 0$) transitions, whereas the ratio is ~ 0.6 for stretched dipole ($\Delta I = 1$) transitions. For mixed ($\Delta I = 1$) transitions, the DCO ratios depend on the the mixing ratio δ, and can therefore be used in favorable cases to deduce the sign of δ, and hence the sign of $(g_K - g_R)/Q_0$ values.

III. RESULTS

The level structure of ^{185}Os was previously investigated by β^+ decay of ^{185}Ir [13], nuclear reactions of ^{185}Os(p,t) [14] and ^{183,186}W(α,xn) [15,16]. In these studies, five one-quasiparticle bands and an $I^\pi = 23/2^-$ isomer were identified. In the present study, most of the known one-quasiparticle bands have been extended to higher spins. In addition, several new high-spin levels including an isomer with $T_{1/2} = 18(2)$ ns have been identified. In Figs. 1 and 2, partial level schemes constructed by the present coincidence data are shown. The one-quasiparticle bands are labeled with likely Nilsson configurations, while the bands newly found in this work are numerically labeled I-IV. The identification of transitions and levels is based on coincidence relationships, γ-ray energy sums, and intensity patterns. Transition energies, relative intensities of γ rays and the initial and final I^π values are listed in Table I. The DCO ratios and the deduced spin differences of the transitions are also given where they were obtained. For $\Delta I = 2$ fast transitions which compete with lower multipole transitions, $E2$ assignments are made since $M2$ assignments for the transitions are not considered due to their small transition probability. Uncertain spin and parity assignments are indicated by brackets in Figs. 1 and 2, and Table I.

A. The $1/2^-[510]$ band

The ground state rotational band based on the $1/2^-[510]$ Nilsson configuration was previously extended as high as $I^\pi = 33/2^-$ [16]. The 3225 keV level was interpreted as an $I^\pi = 31/2^-$ state, decaying into the $I^\pi = 27/2^-$ state at 2571 keV via the 654 keV transition (see Fig. 2). In the present study, an additional decay branch from the 3225 keV level has been observed. A 327 keV transition depopulates the 3225 keV level to a 2898 keV level. Since the 2898 keV level has a high-K configuration, the 3225 keV level is likely interpreted as a multiquasiparticle intrinsic state rather than a member of the ground state band (see also Sec. III I). Four new transitions (642, 659, 664, and 699 keV) including a 642 keV doublet transition have been observed above the 2571 keV. These transitions establish higher-lying levels of the ground state band. DCO ratios are used to deduce spins and parities. The small values of $R_{DCO} = 0.38 - 0.51$ for the $\Delta I = 1$ transitions in this band suggest negative signs for the mixing ratios.

B. The $3/2^-[512]$ band

A 128 keV bandhead and five rotational levels were found previously in the $3/2^-[512]$ band [16]. No new levels have been identified in this study. The $I^\pi = 19/2^-$ level at 1756 keV is strongly populated by the 231 keV $E2$ transition from the $I^\pi = 23/2^-$ level at 1987 keV. The DCO information

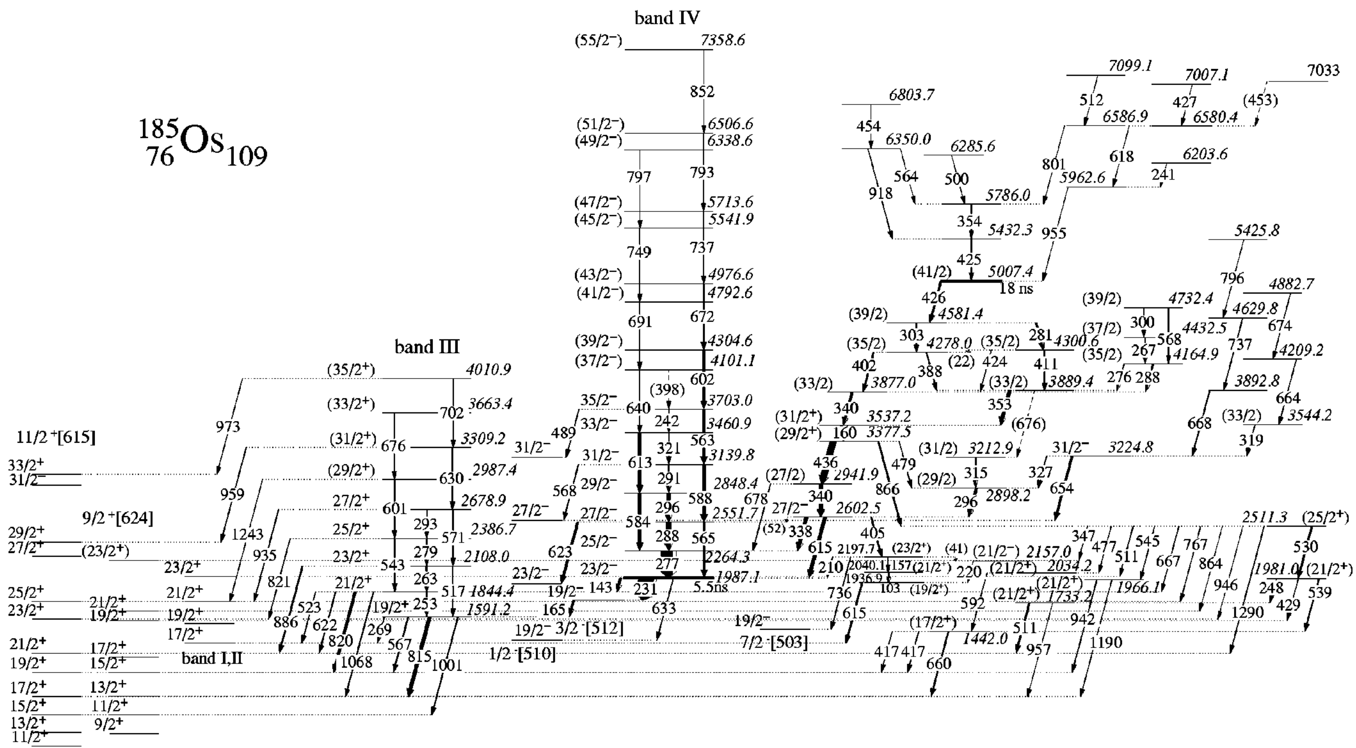

FIG. 2. Partial level scheme showing band III, band IV, and medium- to high-spin states in ^{185}Os. The width of the arrows is proportional to the γ-ray intensities (black) and the calculated intensities of electron conversion (white). Some of the levels in the one-quasiparticle band, and bands I and II are also illustrated.

is consistent with earlier spin and parity assignments [16] of this band. The intense interband transitions from the higher spin states would indicate that this band is not a pure configuration (see Sec. IV D for more details).

C. The 7/2$^-$[503] band

The isomeric level at 102 keV was measured to have $T_{1/2}=3$ μs and was assigned the 7/2$^-$[503] Nilsson configuration [15]. This band is known up to $I^\pi=33/2^-$ for the $\alpha=+1/2$ sequence and $I^\pi=27/2^-$ for the $\alpha=-1/2$ sequence [16]. A level found at 3512 keV has been added to the $\alpha=-1/2$ sequence in this work. DCO ratios confirm the spin and parity assignments, and the small values of $R_{\mathrm{DCO}}=0.18-0.47$ for the $\Delta I=1$ transitions are consistent with negative signs of the mixing ratios.

D. The 9/2$^+$[624] band

The previously identified 9/2$^+$[624] band has been extended as high as $I^\pi=(33/2^+)$ for the $\alpha=+1/2$ sequence and $I^\pi=(23/2^+)$ for the $\alpha=-1/2$ sequence. In addition to the in-band transitions, several interband transitions to the 11/2$^+$[615] band have been observed. DCO ratios for the 177, 623, and 1027 keV transitions and decay properties of the interband transitions support the spin and parity assignments made for the lower-spin states in this band.

E. The 11/2$^+$[615] band

In a previous study [15], the 276 keV isomeric level was measured to have $T_{1/2}=780$ ns, and assigned as the bandhead of the 11/2$^+$[615] band. Levels as high as $I^\pi=41/2^+$ for the $\alpha=+1/2$ sequence and $I^\pi=39/2^+$ for the $\alpha=-1/2$ sequence were previously known [16]. The present data extend this band to $I^\pi=(53/2^+)$. DCO ratios confirm the spin and parity assignments made for this band. The small values of $R_{\mathrm{DCO}}=0.29-0.41$ for the $\Delta I=1$ transitions indicate negative signs for the mixing ratios.

F. Bands I and II

Two bands labeled bands I and II have newly been observed to feed the 11/2$^+$[615] band, forming two different signature sequences. DCO information and decay properties of interband transitions support the spin and parity assignments made for the lower-lying states. From intensities ratios of the $I\rightarrow I$ and $I\rightarrow I-2$ interband transitions, these bands are interpreted as γ-vibrational states coupled to an $i_{13/2}$ neutron, and will be discussed in Sec. IV C 1.

G. Band III based on the 1591 keV level

The $I^\pi=19/2^+$ state at 1591 keV (see Fig. 2) is reported to decay into members of the 11/2$^+$[615] band [16]. A 165 keV transition was also found to connect the 1591 keV level with the $I^\pi=19/2^-$ state in the 3/2$^-$[512] band. The DCO ratio and the intensity balance for the 165 keV transition are consistent with a $\Delta I=0$ $E1$ assignment which confirms the previous $I^\pi=19/2^+$ assignment for the 1591 keV level. A rotational band based on the 1591 keV extending to $I^\pi=(35/2^+)$, and including the previously known [16] I^π

TABLE I. Energies, relative intensities, level assignments, DCO ratios, and multipole assignments for the γ-ray transitions in ^{185}Os. The intensities are relative to the 445.6 keV transition in the $11/2^{+}$[615]band.

E_γ (keV)	I_γ^{a}	E_i (keV)	J_i^π	→	J_f^π	R_{DCO}	ΔI
(22)		4300.6	(35/2)	→	(35/2)		
(38)		38	$3/2^-$	→	$1/2^-$		
(41)		2197.7	$(23/2^-)$	→	$(21/2^-)$		
(52)		2602.5	$27/2^-$	→	$27/2^-$		
(61)		97.5	$5/2^-$	→	$3/2^-$		
90.1(10)	14(4)	127.8	$3/2^-$	→	$3/2^-$		
97.5(1)	49(2)	97.5	$5/2^-$	→	$1/2^-$		
101.1(1)	19(2)	198.1	$7/2^-$	→	$5/2^-$	0.51(3)	1
103.0(10)	2(1)	2040.1	$(21/2^+)$	→	$(19/2^+)$		
119.7(1)	12(1)	317.8	$9/2^-$	→	$7/2^-$	0.43(2)	
126.9(1)	33(6)	402.3	$9/2^+$	→	$11/2^+$		
127.8(10)	7(14)	127.8	$3/2^-$	→	$1/2^-$		
138.7(1)	136(14)	414.3	$13/2^+$	→	$11/2^+$	0.41(1)	1
141.7(1)	6(1)	402.3	$9/2^+$	→	$9/2^-$		
142.7(1)	92(3)	1987.1	$23/2^-$	→	$21/2^+$	0.55(2)	1
151.6(10)	8(1)	1176.7	$17/2^+$	→	$15/2^+$		
151.9(1)	11(1)	1176.7	$17/2^+$	→	$19/2^+$		
157.4(10)	7(1)	2197.7	$(23/2^-)$	→	$(21/2^+)$		
158.2(1)	136(14)	260.6	$9/2^-$	→	$7/2^-$	0.47(1)	1
158.5(1)	54(2)	476.4	$11/2^-$	→	$9/2^-$	0.38(1)	1
159.7(1)	130(4)	3537.2	$(31/2^+)$	→	$(29/2^+)$	0.55(1)	1
160.4(1)	36(4)	198.1	$7/2^-$	→	$3/2^-$		
164.7(1)	73(23)	1755.9	$19/2^-$	→	$19/2^+$	1.1(1)	0
176.1(1)	910(30)	590.4	$15/2^+$	→	$13/2^+$	0.34(1)[b]	1
177.1(10)	16(2)	591.2	$11/2^+$	→	$13/2^+$	0.34(1)[b]	1
178.7(1)	42(1)	1744.3	$25/2^+$	→	$23/2^+$		
185.9(1)	615(19)	776.3	$17/2^+$	→	$15/2^+$	0.30(1)	1
188.2(1)	299(10)	448.7	$11/2^-$	→	$9/2^-$	0.47(1)	1
189.1(1)	79(3)	590.4	$11/2^+$	→	$9/2^+$		
190.8(1)	24(1)	781.6	$13/2^+$	→	$15/2^+$		
191.0(10)	47(2)	781.6	$13/2^+$	→	$11/2^+$		
197.4(1)	181(6)	1222.0	$21/2^+$	→	$19/2^+$	0.40(1)	1
204.8(1)	41(1)	864.8	$15/2^-$	→	$13/2^-$	0.52(1)	1
210.2(10)	198(8)	2197.7	$(23/2^-)$	→	$23/2^-$		
211.4(1)	139(4)	660.2	$13/2^-$	→	$11/2^-$	0.40(1)	1
217.5(1)	171(5)	666.1	$13/2^-$	→	$11/2^-$	0.26(1)	1
220.2(1)	240(9)	317.8	$9/2^-$	→	$5/2^-$	0.91(1)	2
220.3(10)	2(1)	2157.0	$(21/2^-)$	→	$(19/2^+)$	0.78(2)	1
223.8(10)	2(1)	351.5	$7/2^-$	→	$3/2^-$		
231.2()	660(20)	1987.1	$23/2^-$	→	$19/2^-$	0.93(1)	2
236.5(3)	43(1)	1755.9	$19/2^-$	→	$19/2^+$		
236.7(1)	21(1)	1353.5	$19/2^-$	→	$17/2^-$		
241.1(1)	99(3)	907.3	$15/2^-$	→	$13/2^-$	0.25(1)	1
241.9(10)	7(1)	3703.0	$35/2^-$	→	$33/2^-$		
243.3(1)	55(2)	1024.8	$15/2^+$	→	$13/2^+$		
246.8(1)	29(1)	907.3	$15/2^-$	→	$13/2^-$	0.09(1)	1

TABLE I. (*Continued.*)

E_γ (keV)	I_γ^{a}	E_i (keV)	J_i^π	$\rightarrow$	J_f^π	R_{DCO}	ΔI
248.0(10)	10(1)	1981.0	$(21/2^+)$	$\rightarrow$	$(21/2^+)$		
248.1(1)	385(12)	1024.5	$19/2^+$	$\rightarrow$	$17/2^+$	0.29(1)	1
252.9(1)	28(1)	1844.4	$21/2^+$	$\rightarrow$	$19/2^+$		
254.1(1)	9(2)	351.5	$7/2^-$	$\rightarrow$	$5/2^-$		
259.3(2)	4(1)	1929.1	$23/2^-$	$\rightarrow$	$21/2^-$		
263.4(1)	53(2)	2108.0	$23/2^+$	$\rightarrow$	$21/2^+$		
265.9(1)	106(3)	1173.4	$17/2^-$	$\rightarrow$	$15/2^-$	0.19(1)	1
267.4(1)	28(1)	4432.5	$(37/2)$	$\rightarrow$	$(35/2)$		
268.7(1)	24(1)	1591.2	$19/2^+$	$\rightarrow$	$17/2^+$		
275.9(1)	20(1)	4164.9	$(35/2)$	$\rightarrow$	$(33/2)$		
277.1(1)	543(16)	2264.3	$25/2^-$	$\rightarrow$	$23/2^-$	0.37(1)[b]	1
278.4(1)	267(9)	476.4	$11/2^-$	$\rightarrow$	$7/2^-$	0.87(1)[b]	2
278.8(1)	28(1)	2386.7	$25/2^+$	$\rightarrow$	$23/2^+$		
281.0(1)	69(2)	4581.4	$(39/2)$	$\rightarrow$	$(35/2)$	1.2(1)	2
287.5(1)	181(6)	2551.7	$27/2^-$	$\rightarrow$	$25/2^-$	0.33(1)	1
287.6(1)	40(1)	4164.9	$(35/2)$	$\rightarrow$	$(33/2)$	0.58(1)	1
287.8(1)	61(2)	1461.4	$19/2^-$	$\rightarrow$	$17/2^-$	0.32	1
291.3(1)	33(1)	3139.8	$31/2^-$	$\rightarrow$	$29/2^-$		
292.5(1)	11(1)	2678.9	$27/2^+$	$\rightarrow$	$25/2^+$		
296.0(10)	90(3)	2898.2	$(29/2^-)$	$\rightarrow$	$27/2^-$	0.30(1)	1
296.4(1)	124(4)	2848.4	$29/2^-$	$\rightarrow$	$27/2^-$	0.37(1)	1
299.9(1)	12(1)	4732.4	$(39/2)$	$\rightarrow$	$(37/2)$		
300.0(1)	41(7)	402.3	$9/2^+$	$\rightarrow$	$7/2^-$		
303.3(1)	31(1)	4581.4	$(39/2)$	$\rightarrow$	$(35/2)$		
307.8(1)	60(2)	1769.3	$21/2^-$	$\rightarrow$	$19/2^-$	0.18(1)	1
314.6(1)	31(1)	3212.9	$(31/2)$	$\rightarrow$	$(29/2)$		
314.7(1)	513(16)	590.4	$15/2^+$	$\rightarrow$	$11/2^+$	1.0(1)	2
319.3(1)	18(1)	3544.2	$(33/2)$	$\rightarrow$	$31/2^-$	0.25(1)	1
321.0(1)	22(1)	3460.9	$33/2^-$	$\rightarrow$	$31/2^-$		
325.6(1)	37(1)	2095.0	$23/2^-$	$\rightarrow$	$21/2^-$		
326.7(1)	21(1)	3224.8	$31/2^-$	$\rightarrow$	$(29/2^-)$	0.27(1)	1
337.8(1)	131(4)	2602.5	$27/2^-$	$\rightarrow$	$25/2^-$		
339.5(1)	192(6)	2941.9	$(27/2)$	$\rightarrow$	$27/2^-$	1.0(1)	0
339.5(1)	82(3)	3877.0	$(33/2)$	$\rightarrow$	$(31/2^+)$	0.8(1)	1
342.4(1)	410(13)	660.2	$13/2^-$	$\rightarrow$	$9/2^-$	1.0(1)	2
343.4(1)	125(4)	1565.5	$23/2^+$	$\rightarrow$	$21/2^+$	0.28(1)	1
346.2(1)	152(5)	448.7	$11/2^-$	$\rightarrow$	$7/2^-$	0.98(1)	2
346.7(10)	14(1)	2511.3	$(25/2^+)$	$\rightarrow$	$(23/2^+)$		
348.3(1)	59(2)	666.1	$13/2^-$	$\rightarrow$	$9/2^-$		
352.6(1)	122(3)	3889.4	$(33/2)$	$\rightarrow$	$(31/2^+)$	0.52(2)	1
355.1(1)	52(2)	706.6	$11/2^-$	$\rightarrow$	$7/2^-$		
362.1(1)	907(30)	776.3	$17/2^+$	$\rightarrow$	$13/2^+$	1.0(1)	2
375.8(10)	47(2)	1552.2	$19/2^+$	$\rightarrow$	$17/2^+$		
379.4(1)	23(1)	781.6	$13/2^+$	$\rightarrow$	$9/2^+$		
388.3(1)	568(17)	864.8	$15/2^-$	$\rightarrow$	$11/2^-$	1.1(1)	2
388.4(1)	30(1)	4278.0	$(35/2)$	$\rightarrow$	$(33/2)$		
389.0(1)	124(4)	706.6	$11/2^-$	$\rightarrow$	$9/2^-$		

TABLE I. (*Continued.*)

E_γ (keV)	I_γ^a	E_i (keV)	J_i^π	→	J_f^π	R_{DCO}	ΔI
394.5(1)	42(2)	1176.7	$17/2^+$	→	$13/2^+$		
(398)		4101.1	$(37/2^-)$	→	$35/2^-$		
399.6(1)	130(4)	660.2	$13/2^-$	→	$9/2^-$		
400.2(1)	22(1)	1176.7	$17/2^+$	→	$17/2^+$	0.92(1)	0
401.8(10)	49(2)	4278.0	(35/2)	→	(33/2)	0.25(1)	1
402.5(10)	13(1)	1755.9	$19/2^-$	→	$19/2^-$		
405.0(10)	55(2)	2602.5	$27/2^-$	→	$(23/2^-)$		
405.5(1)	185(6)	666.1	$13/2^-$	→	$9/2^-$	1.1(1)	2
411.3()	44(1)	4300.6	(35/2)	→	(33/2)	0.43(1)	1
417.1(10)	26(1)	1442.0	$(17/2^+)$	→	$15/2^+$		
417.4(1)	16(1)	1442.0	$(17/2^+)$	→	$19/2^+$		
423.6(1)	43(2)	1745.4	$21/2^+$	→	$17/2^+$		
424.4(10)	15(1)	4300.6	(35/2)	→	(33/2)	0.71(1)	1
425.0(1)	37(2)	1647.1	$21/2^+$	→	$21/2^+$		
426.0(1)	64(2)	5007.4	(41/2)	→	(39/2)	0.72(3)	1
428.6(10)	11(1)	1981.0	$(21/2^+)$	→	$19/2^+$		
434.0(1)	39(2)	1755.9	$19/2^-$	→	$17/2^+$		
434.1(1)	814(25)	1024.5	$19/2^+$	→	$15/2^+$	1.1(1)	2
434.3(2)	47(2)	1024.8	$15/2^+$	→	$11/2^+$		
435.7(1)	263(8)	3377.5	$(29/2^+)$	→	$(27/2^+)$	0.63(1)	1
445.6(1)	1000(30)	1222.0	$21/2^+$	→	$17/2^+$	1.1(1)	2
450.9(1)	103(3)	1116.8	$17/2^-$	→	$13/2^-$	0.90(2)	2
456.5(1)	512(16)	1116.8	$17/2^-$	→	$13/2^-$	0.90(1)	2
458.8(1)	181(6)	907.3	$15/2^-$	→	$11/2^-$	1.0(1)	2
459.5(1)	42.3(15)	2204.1	$27/2^+$	→	$25/2^+$		
470.1(1)	73(3)	1647.1	$21/2^+$	→	$17/2^+$		
473.0(1)	182(6)	1179.5	$15/2^-$	→	$11/2^-$	1.1(1)	2
477.1(10)	10(1)	2511.3	$(25/2^+)$	→	$(21/2^+)$		
479.3(10)	12(1)	3377.5	$(29/2^+)$	→	$(29/2^-)$		
481.2(1)	69(2)	2000.4	$23/2^+$	→	$19/2^+$		
488.8(1)	597(18)	1353.5	$19/2^-$	→	$15/2^-$	0.96(1)	2
489.4(10)	16(1)	3703.0	$35/2^-$	→	$31/2^-$		
494.9(10)	17(1)	1519.3	$19/2^+$	→	$19/2^+$		
507.4(1)	201(6)	1173.4	$17/2^-$	→	$13/2^-$	1.0(1)	2
511.1(10)	18(1)	2511.3	$(25/2^+)$	→	$23/2^+$		
511.4(10)	64(2)	1733.2	$(21/2^+)$	→	$21/2^+$		
512.9(1)	51(2)	1179.5	$15/2^-$	→	$13/2^-$		
516.8(1)	28(1)	2108.0	$23/2^+$	→	$19/2^+$		
519.5(1)	121(4)	1179.5	$15/2^-$	→	$13/2^-$	0.61(1)	1
522.4(1)	742(22)	1744.3	$25/2^+$	→	$21/2^+$	0.98(1)	2
522.5(10)	24(1)	1844.4	$21/2^+$	→	$17/2^+$		
523.4(1)	31(2)	1745.4	$21/2^+$	→	$21/2^+$		
527.2(1)	55(2)	1552.2	$19/2^+$	→	$19/2^+$		
527.7(1)	49(2)	1552.2	$19/2^+$	→	$15/2^+$		
530.3(1)	68(2)	2511.3	$(25/2^+)$	→	$(21/2^+)$		
535.4(1)	75(3)	2280.6	$25/2^+$	→	$21/2^+$		
539.0(1)	38(1)	1981.0	$(21/2^+)$	→	$(17/2^+)$		

TABLE I. (*Continued.*)

E_γ (keV)	I_γ^{a}	E_i (keV)	J_i^π	→	J_f^π	R_{DCO}	ΔI
541.0(1)	462(14)	1565.5	$23/2^+$	→	$19/2^+$	0.96(1)	2
542.5(1)	40(2)	2386.7	$25/2^+$	→	$21/2^+$		
545.3(10)	12(1)	2511.3	$(25/2^+)$	→	$(21/2^+)$		
553.5(1)	283(9)	1670.2	$21/2^-$	→	$17/2^-$	0.94(1)	2
554.3(1)	190(6)	1461.4	$19/2^-$	→	$15/2^-$	1.1(1)	2
563.0(10)	113(4)	3703.0	$35/2^-$	→	$31/2^-$	1.1(1)	2
565.0(1)	83(3)	2551.7	$27/2^-$	→	$23/2^-$	1.0(1)	2
566.8(1)	45(2)	1591.2	$19/2^+$	→	$19/2^+$		
567.5(10)	8(1)	4732.4	(39/2)	→	(35/2)		
568.4(1)	27(1)	3139.8	$31/2^-$	→	$27/2^-$		
570.8(1)	44(2)	2678.9	$27/2^+$	→	$23/2^+$		
574.9(1)	111(4)	2575.3	$27/2^+$	→	$23/2^+$	1.1(1)	2
575.6(1)	528(16)	1929.1	$23/2^-$	→	$19/2^-$	1.1(1)	2
576.2(1)	348(11)	1755.9	$19/2^-$	→	$15/2^-$	1.1(1)	2
578.0(1)	16(1)	2928.5	$31/2^+$	→	$29/2^+$		
584.5(1)	132(4)	2848.4	$29/2^-$	→	$25/2^-$	1.2(1)	2
586.6(1)	54(3)	1176.7	$17/2^+$	→	$15/2^+$		
588.2(1)	127(4)	3139.8	$31/2^-$	→	$27/2^-$	1.1(1)	2
592.3(1)	15(1)	2034.2	$(21/2^+)$	→	$(17/2^+)$		
595.9(1)	199(6)	1769.3	$21/2^-$	→	$17/2^-$	0.92(2)	2
600.7(1)	45(2)	2987.4	$(29/2^+)$	→	$25/2^+$		
601.6(1)	83(3)	4304.6	$(39/2^-)$	→	$35/2^-$		
601.9(1)	90(3)	2249.1	$25/2^+$	→	$21/2^+$		
604.5(1)	88(3)	2885.1	$(29/2^+)$	→	$25/2^+$		
606.2(1)	497(15)	2350.5	$29/2^+$	→	$25/2^+$	0.97(1)	2
612.2(1)	66(2)	2164.4	$(23/2^+)$	→	$19/2^+$		
612.6(1)	121(4)	3460.9	$33/2^-$	→	$29/2^-$	1.0(1)	2
615.0(1)	56(2)	1936.9	$(19/2^+)$	→	$17/2^+$	0.8(1)	1
615.1(1)	138(4)	2602.5	$27/2^-$	→	$23/2^-$	1.1(1)	2
622.3(1)	30(1)	1844.4	$21/2^+$	→	$21/2^+$		
622.6(1)	59(2)	1647.1	$21/2^+$	→	$19/2^+$	0.44(1)	1
622.8(3)	92(3)	2551.7	$27/2^-$	→	$23/2^-$	0.90(1)	2
630.3(1)	54(2)	3309.2	$(31/2^+)$	→	$27/2^+$		
633.5(1)	20(1)	1987.1	$23/2^-$	→	$19/2^-$	1.0(1)[b]	2
633.8(1)	208(7)	2095.0	$23/2^-$	→	$19/2^-$	1.0(1)[b]	2
634.6(1)	212(7)	2304.8	$25/2^-$	→	$21/2^-$	0.93(1)	2
635.9(1)	59(2)	2885.1	$(29/2^+)$	→	$25/2^+$		
638.8(1)	303(9)	2204.1	$27/2^+$	→	$23/2^+$	1.0(1)	2
639.2(1)	208(6)	1755.9	$19/2^-$	→	$17/2^-$	0.78(1)	1
640.1(1)	38(2)	4101.1	$(37/2^-)$	→	$33/2^-$		
641.7(1)	323(10)	2570.8	$27/2^-$	→	$23/2^-$	1.1(1)[b]	2
642.0(1)	99(3)	3212.9	$31/2^-$	→	$27/2^-$	1.1(1)[b]	2
644.3(1)	99(3)	3219.6	$(31/2^+)$	→	$27/2^+$		
653.9(1)	83(3)	3224.8	$31/2^-$	→	$27/2^-$	1.2(1)	2
658.9(1)	38(1)	3871.6	$(35/2^-)$	→	$31/2^-$		
660.4(10)	46(2)	1442.0	$(17/2^+)$	→	$13/2^+$		
664.1(1)	11(1)	4535.7	$(39/2^-)$	→	$(35/2^-)$		

TABLE I. (*Continued.*)

E_γ (keV)	I_γ^a	E_i (keV)	J_i^π	→	J_f^π	R_{DCO}	ΔI
664.4(1)	13(1)	4209.2		→	(33/2)		
665.4(1)	99(3)	2434.7	$25/2^-$	→	$21/2^-$	1.0(1)	2
667.0(1)	103(3)	3552.1	$(33/2^+)$	→	$(29/2^+)$		
667.1(10)	16(1)	2511.3	$(25/2^+)$	→	$21/2^+$		
668.1(1)	34(1)	3892.8		→	$(31/2^-)$		
672.0(1)	61(2)	4976.6	$(43/2^-)$	→	$(39/2^-)$		
673.5(1)	11(1)	4882.7					
676.0(10)	22(1)	3663.4	$(33/2^+)$	→	$(29/2^+)$		
(676)		3889.4	(33/2)	→	$(31/2^-)$		
677.5(1)	20(1)	2941.9	(27/2)	→	$25/2^-$		
678.8(1)	22(1)	3816.4	$(33/2^-)$	→	$(29/2^-)$		
681.0(1)	12(1)	3718.6	$35/2^+$	→	$33/2^+$		
681.1(10)	6(1)	2885.1	$(29/2^+)$	→	$27/2^+$		
683.6(1)	35(2)	2249.1	$25/2^+$	→	$23/2^+$		
684.1(1)	137(4)	2988.9	$29/2^-$	→	$25/2^-$	1.0(1)	2
685.2(1)	54(2)	3904.7	$(35/2^+)$	→	$(31/2^+)$		
687.0(1)	297(9)	3037.6	$33/2^+$	→	$29/2^+$	1.0(1)	2
691.6(1)	36(1)	4792.6	$(41/2^-)$	→	$(37/2^-)$		
694.5(1)	76(3)	4246.6	$(37/2^+)$	→	$(33/2^+)$		
694.8(1)	85(3)	2789.9	$27/2^-$	→	$23/2^-$	0.92(1)	2
699.0(1)	13(1)	5234.7	$(43/2^-)$	→	$(39/2^-)$		
701.8(1)	14(1)	4010.9	$(35/2^+)$	→	$(31/2^+)$		
702.9(1)	49(2)	3137.6	$(29/2^-)$	→	$25/2^-$		
705.4(1)	36(1)	3694.3	$33/2^-$	→	$29/2^-$		
714.9(1)	109(4)	2280.6	$25/2^+$	→	$23/2^+$	0.15(1)	1
719.7(1)	49(2)	2968.9	$(29/2^+)$	→	$25/2^+$		
720.8(1)	116(4)	1745.4	$21/2^+$	→	$19/2^+$	0.39(1)	1
721.6(1)	21(1)	3511.5	$(31/2^-)$	→	$27/2^-$		
724.5(1)	214(7)	2928.5	$31/2^+$	→	$27/2^+$	0.93(1)	2
731.4(1)	149(5)	1321.9	$17/2^+$	→	$15/2^+$	0.45(1)	1
731.5(1)	46(2)	5284.9	$45/2^+$	→	$41/2^+$	0.83(2)	2
734.0(10)	14(1)	4428.3	$(37/2^-)$	→	$33/2^-$		
736.3(1)	23(1)	2197.7	$(23/2^-)$	→	$19/2^-$		
736.9(1)	26(1)	5713.6	$(47/2^-)$	→	$(43/2^-)$		
737.0(10)	17(1)	4629.8					
742.7(1)	15(1)	4647.2	$(39/2^+)$	→	$(35/2^+)$		
742.9(1)	119(4)	1519.3	$19/2^+$	→	$17/2^+$	0.34(1)	1
743.3(1)	11(1)	6017.5	$(47/2^+)$	→	$(43/2^+)$		
746.0(1)	32(1)	5274.2	$(43/2^+)$	→	$39/2^+$		
749.3(1)	27(1)	5541.9	$(45/2^-)$	→	$(41/2^-)$		
749.4(1)	167(5)	3787.0	$37/2^+$	→	$33/2^+$	1.0(1)	2
760.8(1)	24(1)	6045.7	$(49/2^+)$	→	$45/2^+$		
762.7(1)	27(2)	1176.7	$17/2^+$	→	$13/2^+$		
764.8(10)	28(11)	2968.9	$(29/2^+)$	→	$27/2^+$		
766.4(1)	75(3)	4553.4	$41/2^+$	→	$37/2^+$	0.82(2)	2
767.2(10)	9(1)	2511.3	$(25/2^+)$	→	$25/2^+$		
776.0(10)	11(1)	5204.3	$(41/2^-)$	→	$(37/2^-)$		

TABLE I. (*Continued.*)

E_γ (keV)	I_γ^a	E_i (keV)	J_i^π	$\rightarrow$	J_f^π	R_{DCO}	ΔI
778.3(1)	114(4)	2000.4	$23/2^+$	$\rightarrow$	$21/2^+$	0.23(1)	1
790.1(1)	134(4)	3718.6	$35/2^+$	$\rightarrow$	$31/2^+$	1.0(1)	2
793.1(1)	12(1)	6506.6	$(51/2^-)$	$\rightarrow$	$(47/2^-)$		
796.0(10)	4(1)	5425.8					
796.7(1)	9(1)	6338.6	$(49/2^-)$	$\rightarrow$	$(45/2^-)$		
809.6(1)	72(2)	4528.2	$39/2^+$	$\rightarrow$	$35/2^+$	1.1(1)	2
814.9(1)	142(5)	1591.2	$19/2^+$	$\rightarrow$	$17/2^+$	0.49(1)	1
818.1(2)	4(1)	6835.6	$(51/2^+)$	$\rightarrow$	$(47/2^+)$		
819.9(1)	105(3)	1844.4	$21/2^+$	$\rightarrow$	$19/2^+$	0.33(1)	1
821.2(1)	17(1)	2386.7	$25/2^+$	$\rightarrow$	$23/2^+$	0.15(1)	1
831.1(1)	49(2)	2575.3	$27/2^+$	$\rightarrow$	$25/2^+$	0.21(1)	1
838.1(1)	13(1)	3806.9	$(33/2^+)$	$\rightarrow$	$(29/2^+)$		
839.9(1)	10(1)	6885.6	$(53/2^+)$	$\rightarrow$	$(49/2^+)$		
852.0(10)	3(1)	7358.6	$(55/2^-)$	$\rightarrow$	$(51/2^-)$		
859.5(1)	6(1)	4647.2	$(39/2^+)$	$\rightarrow$	$37/2^+$		
860.9(5)	8(1)	2789.9	$27/2^-$	$\rightarrow$	$23/2^-$		
864.4(10)	5(1)	2511.3	$(25/2^+)$	$\rightarrow$	$21/2^+$		
866.0(1)	54(1)	3377.5	$(29/2^+)$	$\rightarrow$	$(25/2^+)$	1.1(2)	2
866.3(1)	5(1)	3904.7	$(35/2^+)$	$\rightarrow$	$33/2^+$		
869.2(1)	29(1)	3219.6	$(31/2^+)$	$\rightarrow$	$29/2^+$	0.48(1)	1
871.1(1)	65(2)	1647.1	$21/2^+$	$\rightarrow$	$17/2^+$		
878.4(10)	5(1)	3806.9	$(33/2^+)$	$\rightarrow$	$31/2^+$		
886.1(1)	52(2)	2108.0	$23/2^+$	$\rightarrow$	$21/2^+$	0.29(1)	1
907.8(1)	76(3)	1321.9	$17/2^+$	$\rightarrow$	$13/2^+$		
928.9(2)	6(1)	4647.2	$(39/2^+)$	$\rightarrow$	$35/2^+$		
929.1(1)	63(2)	1519.3	$19/2^+$	$\rightarrow$	$15/2^+$	0.90(1)	2
934.7(1)	25(1)	2678.9	$27/2^+$	$\rightarrow$	$25/2^+$		
941.7(1)	23(1)	1966.1	$(21/2^+)$	$\rightarrow$	$19/2^+$		
946.0(10)	5(1)	2511.3	$(25/2^+)$	$\rightarrow$	$23/2^+$		
956.9(10)	6(1)	1733.2	$(21/2^+)$	$\rightarrow$	$17/2^+$		
958.6(1)	21(1)	3309.2	$(31/2^+)$	$\rightarrow$	$29/2^+$		
969.3(1)	37(2)	1745.4	$21/2^+$	$\rightarrow$	$17/2^+$		
973.2(1)	8(1)	4010.9	$(35/2^+)$	$\rightarrow$	$33/2^+$		
976.0(1)	15(1)	2000.4	$23/2^+$	$\rightarrow$	$19/2^+$		
976.1(3)	4(1)	3904.7	$(35/2^+)$	$\rightarrow$	$31/2^+$		
1001.1(1)	33(1)	1591.2	$19/2^+$	$\rightarrow$	$15/2^+$		
1027.2(1)	48(2)	2249.1	$25/2^+$	$\rightarrow$	$21/2^+$	0.92(2)	2
1068.4(1)	32(1)	1844.4	$21/2^+$	$\rightarrow$	$17/2^+$		
1141.5(1)	17(1)	2885.1	$(29/2^+)$	$\rightarrow$	$25/2^+$		
1189.5(2)	10(1)	1966.1	$(21/2^+)$	$\rightarrow$	$17/2^+$		
1201.6(2)	5(1)	3552.1	$(33/2^+)$	$\rightarrow$	$29/2^+$		
1209.1(10)	2(1)	4246.6	$(37/2^+)$	$\rightarrow$	$33/2^+$		
1224.8(1)	11(1)	2968.9	$(29/2^+)$	$\rightarrow$	$25/2^+$		
1242.6(2)	8(1)	2987.4	$(29/2^+)$	$\rightarrow$	$25/2^+$		
1289.5(10)	20(1)	2511.3	$(25/2^+)$	$\rightarrow$	$21/2^+$		
1455.8(4)	3(1)	3806.9	$(33/2^+)$	$\rightarrow$	$29/2^+$		

TABLE I. (*Continued.*)

E_γ (keV)	I_γ^{a}	E_i (keV)	J_i^π	→	J_f^π	R_{DCO}	ΔI
Transitions above the 5007 keV isomer[c]							
241.0(1)	35(6)	6203.6					
353.7(1)	473(31)	5786.0					
424.9(1)	1000(50)	5432.3					
426.8(2)	41(18)	7007.1					
(453)		7033					
453.7(1)	180(26)	6803.7					
499.7(1)	207(26)	6285.6					
512.4(1)	198(24)	7099.1					
564.0(1)	99(9)	6350.0					
617.8(1)	153(20)	6580.4					
800.8(1)	208(23)	6586.9					
917.8(1)	126(18)	6350.0					
955.2(1)	303(27)	5962.6					

[a] γ-ray intensities are normalized to the 445.6 keV transition.
[b] Doublet transitions.
[c] γ-ray intensities are normalized to the 424.9 keV transition.

$=21/2^+$ and $23/2^+$ levels has newly been established. The lower-lying levels in this band are connected by weak $M1(+E2)$ transitions. Decay properties of interband transitions and DCO ratios are used to deduce the spins and parities of this band. From the decay curve analysis, an upper limit of 5 ns was deduced for the half-life of the 1591 keV bandhead.

H. Band IV based on the 1987 keV level

The 1987 keV isomeric level with $T_{1/2}=5.5(10)$ ns was reported to decay into the $I^\pi=19/2^-$ level in the $3/2^-[512]$ band via a 231 keV $E2$ transition, and into the $I^\pi=21/2^+$ state in the band III via a 143 keV transition [16]. In the present work, a 634 keV transition has been observed to depopulate the 1987 keV level into the $I^\pi=19/2^-$ level in the $1/2^-[510]$ band. The previous assignment of $\Delta I=1$ $E1$ for the 143 keV transition is confirmed by the DCO information and the γ-ray intensity balance, and supports the assignment of $I^\pi=23/2^-$ for the 1987 keV level.

The $I^\pi=25/2^-$, $27/2^-$, and $29/2^-$ levels at excitation energies of 2264, 2603, and 2942 keV, associated with 277, 338, 340, and 615 keV transitions, were previously placed as rotational band members based on the 1987 keV level [16]. However, the present analysis of the coincidence data results in a different placement of the 2603 and 2942 keV levels. In Fig. 3, γ-ray lines at 277, 288, and 296 keV as well as the corresponding crossover transitions (565 and 585 keV) can be seen. These transitions now establish the $I^\pi=25/2^-$ and $27/2^-$ rotational levels at 2552 and 2848 keV built on the 5.5 ns isomeric state instead of the 2603 and 2942 keV levels. The present coincidence data also reveal additional decay branches from the 2603 keV level via a 405 keV transition and an unobserved 52 keV transition. Furthermore, a 678 keV transition has been found to depopulate the 2942 keV level. The DCO ratio for the 615 keV transition is consistent with an assignment of $\Delta I=2$, resulting in the $I^\pi=27/2^-$ assignment for the 2603 keV level. For the 340 keV transition, the DCO ratio agrees with an assignment of either $\Delta I=0$ or 2. However, the presence of the 678 keV transition which feeds the $I^\pi=25/2^-$ level in band IV rejects an assignment of $\Delta I=2$ for the following reason. A $\Delta I=2$ assignment gives spin and parity $I=31/2$ to the 2942 keV level which then requires a spin change of $3\hbar$ for the 678 keV transition. An $E3$ or $M3$ transition should hardly occur at all with the 340 keV fast $M2$ or $E2$ transition in the present case. Consequently, the assignment of $\Delta I=0$ for the 340 keV transition, i.e., $I=27/2$ for the 2942 keV level is preferred.

For higher spins of band IV, levels extending as high as $I^\pi=(49/2^-)$ for the $\alpha=+1/2$ sequence and $I^\pi=(55/2^-)$ for the $\alpha=-1/2$ sequence have been observed. Three interband $\Delta I=2$ transitions (489, 568, and 623 keV) to the $1/2^-[510]$

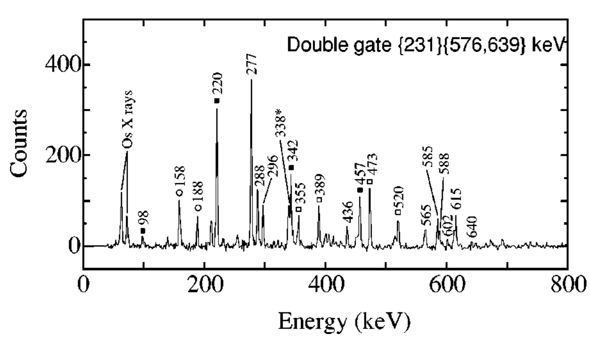

FIG. 3. Coincidence spectrum double gated on the 231 and 576, 639 keV γ-ray combination, showing transitions above the $I^\pi=23/2^-$ state at 1987 keV. Transitions in (or from) the $1/2^-[510]$, $3/2^-[512]$, and $7/2^-[503]$ bands are marked by filled squares, open squares, and open circles, respectively. Transition energies of doublets or higher degeneracies are suffixed by asterisks.

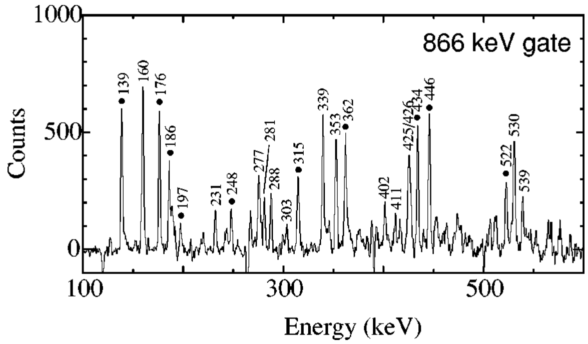

FIG. 4. Coincidence spectrum gated on the 866 keV $(29/2^+) \to (25/2^+)$ transition. Transitions in the $11/2^+[615]$ bands are marked by filled circles.

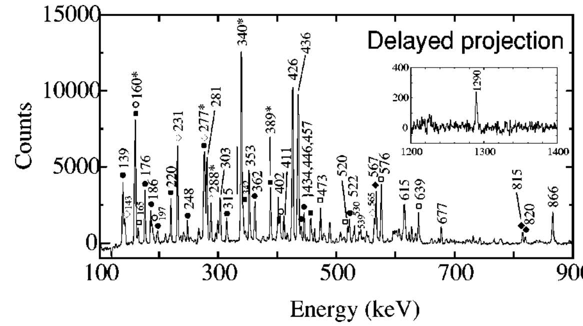

FIG. 5. Delayed γ-ray spectrum gated on the sum of the 425, 801, 918, and 955 keV transitions, showing γ rays below the $I^\pi = (41/2)$ isomer. Transitions in the $1/2^-[510]$, $3/2^-[512]$, $7/2^-[503]$, and $11/2^+[615]$ bands, band III, and band IV are marked by filled squares, open squares, open circles, filled circles, filled diamonds, and open diamonds, respectively. Transition energies of doublets or higher degeneracies are suffixed by asterisks.

band have also been found. The DCO information and the observation of both the cascade and the corresponding crossover transitions are used to deduce spins and parities of this band. The small DCO ratios for the $\Delta I = 1$ transitions indicate negative signs of the mixing ratios.

I. Medium- to high-spin states

As mentioned in Sec. III A, the 3225 keV level is depopulated by the 327 and 654 keV transitions. The 2898 keV level populated by the 327 keV transition decays into the $I^\pi = 27/2^-$ level at 2603 keV via a 296 keV transition. The DCO ratios of the 296, 327, and 654 keV transitions are consistent with the spin and parity assignment of $I^\pi = 31/2^-$ for the 3225 keV level. The presence of the 327 keV transition would indicate that the 3225 keV state has a multiquasiparticle character despite its direct decay to the $I^\pi = 27/2^-$ level in the ground state rotational band. Several levels have been placed above the 3225 keV level. However, spins and parities are not given to these levels due to lack of the DCO information except for the 319 keV transition.

A 3378 keV level has newly been found to decay into the 2942 keV level via a 436 keV transition. The DCO ratio for this transition suggests $I = 29/2$ for the 3378 keV level. This level is also depopulated by a 866 keV transition which establishes a 2511 keV level. The intensity of γ rays below the 2511 keV level is too weak to extract DCO ratios. However, together with the $I = 29/2$ assignment for the 3378 keV level, the presence of 667, 864, and 1290 keV transitions depopulating the 2511 keV level to the $I^\pi = 21/2^+$ states in the bands III, $9/2^+[624]$, and $11/2^+[615]$ suggests that all these transitions as well as the 866 keV transition have stretched quadrupole $(\Delta I = 2)$ character which would explain the spin change of $4\hbar$ by the two consecutive transitions. We therefore assign $I^\pi = (25/2^+)$ and $(29/2^+)$ for the 2511 and 3378 keV levels. Through similar considerations, spin and parity assignments have been made for 1442, 1966, 1981, and 2034 keV levels.

Above the 3378 keV level, several new levels have been observed. Most of the levels are populated through the decay of a new high-spin isomer (see also Sec. III J). Figure 4 shows the γ-ray spectrum gated by the 866 keV transition. An intense 160 keV transition depopulates a 3537 keV level into the 3378 keV level. The total conversion coefficient of the 160 keV transition is deduced to be $\alpha_{\text{tot}} = 0.97(2)$ from the γ-ray intensity balance at the 3378 keV level. Comparison with the calculated values [17] of $\alpha_{\text{tot}} = 0.12$ (where the transitions is $E1$), $1.5(M1)$, and $0.74(E2)$ supports a mixed $M1 + E2$ assignment for the 160 keV transition. The DCO information is also consistent with the $\Delta I = 1$ assignment. The 3537 keV level is therefore assigned to be $I^\pi = (31/2^+)$. The level ordering and the assignments of spin and parity for the higher-lying levels are based on the γ-ray relative intensities and the DCO ratios.

J. New high-spin isomer at 5007 keV

From analysis of delayed coincidence data, a new high-spin isomer has been identified at 5007 keV. Figure 5 shows a γ-ray spectrum for transitions below the isomer. In addition to the transitions in the one-quasiparticle bands, band III and band IV, the 866 keV transition as well as the coincident γ rays (see Fig. 4) can be seen. The decay of the isomer is most intensely carried out by the 426 and 160 keV transitions to the 4581 and 3537 keV levels. Between these two levels, γ-ray intensity is dispersed among several transitions.

For the determination of the half-life of the 5007 keV isomer, time difference spectra between transitions above and below the isomer have been analyzed. Figure 6 illustrates a decay curve for the 5007 keV isomer. By fitting the slope of the decay curve, the half-life of the 5007 keV isomer has been obtained as $T_{1/2} = 18(2)$ns.

Above the 5007 keV isomer, several transitions have been identified as seen in Fig. 7. No regular band structure is apparent. The level placement is based on the relative intensities of the transitions. Information on the transitions above the isomers is presented in the end of Table I.

IV. DISCUSSION

A. Alignments

In the cranked shell model [18], rotational alignments i can be obtained by subtracting aligned angular momenta of

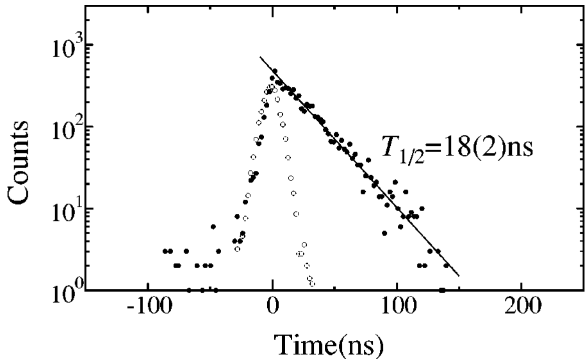

FIG. 6. Time difference spectrum between the 955 keV transitions and the 340, 353, 426, 436 keV transitions is shown with filled circles. The time difference spectrum in prompt coincidence between the 522 and 446 keV transitions is also shown with open circles.

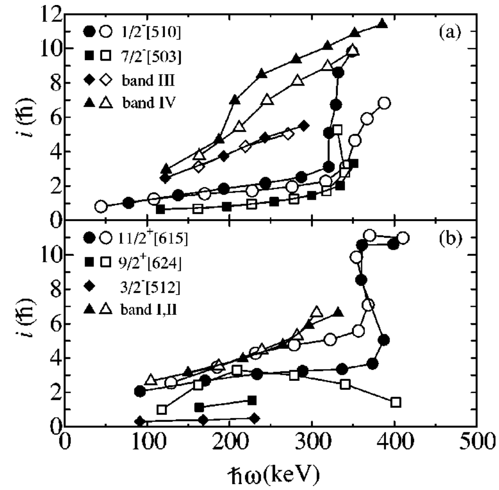

FIG. 8. Alignments for the $1/2^-[510]$ (open and filled circles), $7/2^-[503]$ bands (open and filled squares), band III (open and filled diamonds), and band IV (open and filled triangles) are plotted in upper panel (a), while those for the $11/2^+[615]$ (open and filled circles), $9/2^+[624]$ (open and filled squares), $3/2^-[512]$ (open diamond), and bands I, II (open and filled triangles) are plotted in lower panel (b). The $\alpha=+1/2$ and $-1/2$ sequences are shown with open and filled symbols, respectively. Harris parameters of $\mathfrak{J}_0=24$ MeV^{-1} $\hbar^2$ and $\mathfrak{J}_1=66$ MeV^{-3} $\hbar^4$ are used.

the reference configuration from total aligned angular momenta $I_x[=\sqrt{I(I+1)-K^2}]$. For odd-mass nuclei, the ground state bands in neighboring even-even nuclei are used for the reference. In Fig. 8, the rotational alignments for the bands observed in ^{185}Os are shown as a function of rotational frequencies $\hbar\omega$ in units of keV. Harris parameters of $\mathfrak{J}_0=24$ MeV^{-1} $\hbar^2$ and $\mathfrak{J}_1=66$ MeV^{-3} $\hbar^4$ are obtained by averaging the values for the ground state bands in ^{184}Os [2] and ^{186}Os [19]. In the calculation, we assume the K quantum numbers fixed at the bandhead spin values.

The $1/2^-[510]$, $3/2^-[512]$, and $7/2^-[503]$ bands show small alignments at low rotational frequencies which are consistent with the systematic behavior of nonaligned one-quasiparticle bands in the region. For the $1/2^-[510]$ and $7/2^-[503]$ bands, rapid increases in the alignments are observed at $\hbar\omega=330-340$ keV, which can be understood as a result of the band crossings with aligned three-quasiparticle bands (s bands). The crossing frequencies of $\hbar\omega=330-340$ keV are about 110–120 keV larger than that for the $7/2^-[503]$ band in ^{183}Os ($\hbar\omega_{AB}\approx 220$ keV) [20]. This can be attributed to the presence of a minor shell closure at $N=108$ which increases the quasiparticle energy of the $i_{13/2}$ orbital at zero rotational frequency and in turn causes delayed AB band crossing. Similar phenomena are observed in the neighboring even-even nuclei with $N=108$, ^{182}W [21] and ^{184}Os [22]. For the $11/2^+[615]$ band, the alignment is about $2\hbar$ in both the signature sequences. The large signature splitting and the large crossing frequencies (BC and AD band crossings) result from the blocking effect for the $i_{13/2}$ neutron orbital. Note that the notations A,B,C, and D are prescribed by Ref. [18].

The magnitude of alignments for multiquasiparticle bands is the sum of those of the constituent quasiparticles. Therefore, for bands which involve $i_{13/2}$ neutrons and/or $h_{9/2}$ protons, large rotational alignments are expected due to the strong Coriolis interaction on these quasiparticles (see, e.g., Ref. [23]). This can be used in quasiparticle configuration assignments for the bands observed in ^{185}Os.

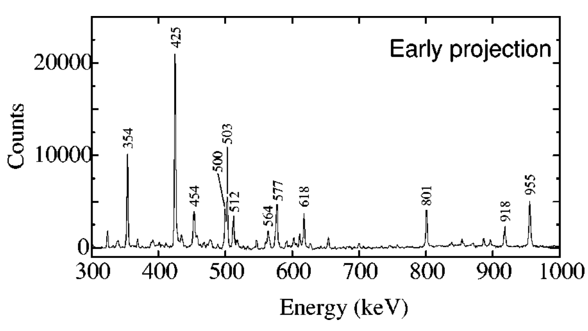

FIG. 7. Early projection gated on the delayed 340, 353, 426, and 436 keV transitions, showing the transitions above the $I^\pi=(41/2)$ isomer.

B. g_K factors

Intensity ratios between $\Delta I=1$ cascade and $\Delta I=2$ crossover transitions in a band can be used in the asymptotic limit to deduce g_K factors. In the rotational model [24], mixing ratios δ and g_K factors are deduced as

$$\frac{\delta^2}{1+\delta^2}=\lambda\frac{E_\gamma^5(I\to I-1)}{E_\gamma^5(I\to I-2)}\frac{\langle I\ K\ 2\ 0|I-1\ K\rangle^2}{\langle I\ K\ 2\ 0|I-2\ K\rangle^2} \qquad (1)$$

and

TABLE II. g_K values deduced from the branching ratios for the bands in ^{185}Os.

Band	I_i	$E_\gamma(E2)$ (keV)	$E_\gamma(M1/E2)$ (keV)	λ	$(g_K^{exp}-g_R)$[a]	$(g_K^{cal}-g_R)$[b]
$1/2^-[510]$	5/2	160.4	101.1	1.97(30)	−0.96(8)	−1.70
	7/2	220.2	119.7	19.9(12)	−0.55(1)	−1.70
	9/2	278.4	158.5	4.94(23)	−1.42(3)	−1.70
	15/2	388.3	204.8	13.8(6)	−1.37(3)	−1.70
	19/2	488.8	236.7	28.9(14)	−1.36(3)	−1.70
	23/2	575.6	259.3	150(18)	−0.78(5)	−1.70
$7/2^-[503]$	11/2	346.2	188.2	0.51(2)	−0.52(1)	−0.54
	13/2	405.5	217.5	1.09(5)	−0.52(1)	−0.54
	15/2	458.8	241.1	1.83(8)	−0.52(1)	−0.54
	17/2	507.4	265.9	1.90(9)	−0.61(2)	−0.54
	19/2	554.3	287.8	3.13(15)	−0.54(1)	−0.54
	21/2	595.9	307.8	3.32(15)	−0.58(2)	−0.54
	23/2	633.8	325.6	5.56(27)	−0.49(1)	−0.54
$9/2^+[624]$	13/2	379.4	191.0	0.50(3)	−0.46(2)	−0.25
	15/2	434.3	243.3	0.85(5)	−0.43(1)	−0.29
	17/2	394.5	151.6	5.42(36)	−0.31(1)	−0.31
	19/2	527.7	375.8	1.05(6)	−0.36(1)	−0.33
$11/2^+[615]$	15/2	314.7	176.1	0.56(2)	−0.21(1)	−0.23
	17/2	362.1	185.9	1.47(6)	−0.23(1)	−0.26
	19/2	434.1	248.1	2.12(9)	−0.20(1)	−0.28
	21/2	445.6	197.4	5.54(24)	−0.23(1)	−0.30
	23/2	541.0	343.4	3.71(16)	−0.16(1)	−0.31
	25/2	522.4	178.7	17.6(8)	−0.25(1)	−0.31
	27/2	638.8	459.5	7.15(34)	[c]	−0.32
	31/2	724.5	578.0	13.5(8)	[c]	−0.32
	35/2	790.1	681.0	11.3(7)	[c]	−0.33
Band III[d]	23/2	516.8	263.4	0.52(3)	±0.19(1)	−0.22
	25/2	542.5	278.8	1.42(9)	±0.15(1)	−0.24
	27/2	570.8	292.5	3.92(29)	±0.08(1)	−0.26
Band IV[d]	27/2	565.0	287.5	0.46(2)	−0.17(1)	−0.08
	29/2	584.5	296.4	1.07(5)	−0.15(1)	−0.12
	31/2	588.2	291.3	3.88(18)	−0.06(1)	−0.15
	33/2	612.6	321.0	5.56(27)	−0.01(2)	−0.17
	35/2	563.0	241.9	15.2(12)	−0.04(1)	−0.20

[a] $Q_0=5.7$ e b is used.
[b] The calculated values have uncertainties of ±0.05 propagated from the assumption of $g_R=0.20\pm0.05$.
[c] The negative values of δ^2 are obtained in Eq. (1). This may indicate that the assumption of the strong coupling limit to derive Eq. (1) is not appropriate for describing these states.
[d] $K=19/2$ for band III and $K=23/2$ for band IV are assumed (see Sec. IV C).

$$\frac{(g_K-g_R)^2}{Q_0^2}=0.289\frac{E_\gamma^2(I\rightarrow I-1)}{\delta^2K^2}\frac{\langle I\ K\ 2\ 0|I-1\ K\rangle^2}{\langle I\ K\ 1\ 0|I-1\ K\rangle^2} \quad (2)$$

with the transition energies in MeV, where λ is the intensity ratio $T_\gamma(I\rightarrow I-2)/T_\gamma(I\rightarrow I-1)$, g_R the gyromagnetic ratio for the collective rotation, and Q_0 the intrinsic quadrupole moment. The experimental (g_K-g_R) values extracted from the above equations are listed in Table II. When the signs of the mixing ratios are not known from the DCO information, the possible two values of (g_K-g_R) are listed. Here, we used

TABLE III. g_{K_j} factors and alignments of the single-particle orbitals considered for ^{185}Os.

Neutrons	g_{K_j}	i_j	Protons	g_{K_j}	i_j
$1/2^-[510]$	−1.50	0.0	$1/2^-[541]$	0.76	3.5
$1/2^-[521]$	0.64	0.0	$5/2^+[402]$	1.57	0.0
$3/2^-[512]$	0.54	0.0	$7/2^+[404]$	0.63	0.0
$7/2^-[503]$	−0.34	0.0	$9/2^-[514]$	1.30	0.5
$9/2^+[624]$	−0.23	2.0			
$11/2^+[615]$	−0.18	2.0			

$Q_0=5.7$ *e* b obtained by averaging $Q_0=5.67$ *e* b for ^{184}Os [2] and $Q_0=5.7$ *e* b for ^{186}Os [19].

The effective g_K factors [25] can be calculated in the semiclassical model [26] by the following equation:

$$g_K^{\text{eff}} - g_R = \frac{\Sigma(g_{K_j} - g_R)K_j}{K} - \frac{\Sigma(g_{K_j} - g_R)i_j}{\sqrt{I^2 - K^2}}, \qquad (3)$$

where g_{K_j} is the gyromagnetic factor of the jth quasiparticle, i_j the aligned angular momentum, K_j the angular momentum projection on the deformation axis, and $K=\Sigma K_j$. The first term represents the usual expression of (g_K-g_R) in the strong coupling limit, while the second term is due to the Coriolis effects which are important for configurations involving $i_{13/2}$ neutrons and/or $h_{9/2}$ protons in the present case. The i_j values were taken from the known one-quasiparticle bands of odd-*A* nuclei in this mass region. The g_{K_j} factors for each quasiparticle have been calculated using the formula

$$g_{K_j} = (\langle l_3\rangle g_l + \langle s_3\rangle g_s)/K_j \qquad (4)$$

assuming 70% of the free nucleon g_s factors [27] ($g_s^{\text{free}}=5.59$ for protons and −3.83 for neutrons). Here, l_3 (s_3) is the component of the orbital angular momentum (intrinsic spin) projected on the nuclear symmetry axis, and $g_l=1$ for protons, $g_l=0$ for neutrons. The expectation values of s_3 were obtained from Nilsson wave functions. Table III summarizes the g_{K_j} factors and the alignments i_j used in the calculation. The calculated (g_K-g_R) values are also shown in Table II.

C. Band properties and configuration assignments

In this section, quasiparticle configurations for bands I–IV are discussed by comparison between the observed and predicted alignments and g_K factors. We estimated excitation energies (E_x^{cal}) of multiquasiparticle states by summing the energies of the constituent single quasiparticle states and the energies needed to break the quasiparticle pairs. The excitation energies of the one-quasiparticle states in ^{185}Os, ^{183}Re, and ^{185}Re are taken from Ref. [28]. Averages of ^{183}Re and ^{185}Re were used in the calculation for protons. The neutron and proton pairing gap energies ($\Delta_n=706$ and $\Delta_p=834$ keV) were obtained by averaging those for ^{184}Os and ^{186}Os using the third order odd-even mass differences [29], and they were reduced by 20% for each quasiparticle broken pair to account for the weaker pair field in the multiquasiparticle configurations. Since the residual interaction defined by the empirical Gallagher-Moszkowski (GM) rules [30] is important to calculate excitation energies of multiquasiparticle states, the associated GM splitting energies E^{GM} taken from Ref. [31] are added to the calculated excitation energies E_x^{cal}.

1. Bands I and II

Bands I and II gain two units of alignment in the rotational frequency range of 100–300 keV [see Fig. 8(b)], indicating that the configuration involves one or more alignable quasiparticles. Since these bands predominantly decay to members of the $11/2^+[615]$ band and have similar alignment behavior to the $11/2^+[615]$ band, the aligned quasiparticle is plausibly the $11/2^+[615]$ neutron. The interband transitions to the $11/2^+[615]$ band from band I and II also suggest an admixture of the $11/2^+[615]$ component in the configuration. In the neighboring even-even nuclei ^{182}Os [32,33], ^{184}Os [2] and ^{186}Os [19], low-lying γ-vibrational bands based on the 891, 943, and 768 keV levels are known to decay to the ground state bands by both $\Delta I=2$ and 0 transitions. Assuming the $I\rightarrow I$ transitions to be of *E*2 character, the measured $B(E2)$ ratios of the $I\rightarrow I$ and $I\rightarrow I-2$ transitions are 6.3(5) and 18(2) at $I^\pi=19/2^+$ and $21/2^+$ for ^{185}Os. These can be compared to values of 2.3(2), 1.9(2), 2.4(1) at $I_\gamma^\pi=2^+$, and 7.7(15), 5.1(4), 11(3) at $I_\gamma^\pi=4^+$ for ^{182}Os [34], ^{184}Os [34], ^{186}Os [19], respectively, and 15(1) at $I_\gamma^\pi=6^+$ for ^{186}Os [19]. Note that the $I^\pi=19/2^+$ state in ^{185}Os corresponds to $I_\gamma^\pi=4^+$ in the even-even Os nuclei, and the transitions between the γ-band and ground state rotational band in ^{182}Os have large *E*2 components [33]. Although a three-quasiparticle configuration cannot be completely excluded, the assignment of the γ phonon $\otimes 11/2^+[615]$ for bands I and II is preferred. A similar band is observed in ^{183}Os [20].

2. Band III

The bandhead spin and parity have been assigned to be $I^\pi=19/2^+$. The excitation energy of 1591 keV requires excitation of three quasiparticles with at least one alignable quasiparticle to account for the alignment [see Fig. 8(a)]. The following configurations give low-lying $K^\pi=19/2^+$ states:

$$K^\pi = 19/2_1^+, \nu\{3/2^-[512]7/2^-[503]9/2^+[624]\},$$

$$E_x^{\text{cal}} + E^{\text{GM}} = 1763 - 150 = 1613 \text{ keV},$$

$$K^\pi = 19/2_2^+, \nu\{1/2^-[521]7/2^-[503]11/2^+[615]\},$$

$$E_x^{\text{cal}} + E^{\text{GM}} = 1915 - 150 = 1765 \text{ keV}.$$

The expected $(g_K^{\text{cal}}-g_R)$ values are −0.28(5) and −0.22(5) at $I^\pi=23/2^-$ for the $K^\pi=19/2_1^+$ and $K^\pi=19/2_2^+$ configurations, respectively, which are consistent with one of the measured values ($g_K^{\text{exp}}-g_R=-0.19$). Since band III decays predominantly to the $11/2^+[615]$ band rather than the $9/2^+[624]$ band, the $K^\pi=19/2_2^+$ configuration is preferred.

Although the present experimental data cannot exclude the possibility of a positive $(g_K^{\rm exp}-g_R)$ value, three quasiparticle $K^\pi=19/2^+$ configurations including more than one quasiproton that can give the positive (g_K-g_R) values are expected at higher excitation energies.

3. Band IV

The bandhead spin and parity have been determined to be $I^\pi=23/2^-$. Previously, the $\nu 3/2^-[512]\otimes\pi\{9/2^-[514]11/2^-[505]\}$ configuration was assigned to this band based on the agreement between the measured and predicted g_K factors $(g_K-g_R=0.76)$ [16]. Since the present level scheme differs from that of Ref. [16], the configuration should be reexamined. In the present data, negative $(g_K^{\rm exp}-g_R)$ values are obtained, which are consistent with a three-quasineutron configuration rather than the two-quasiproton and one-quasineutron configuration proposed previously. The only configuration giving a low-lying three-quasineutron state in ^{185}Os is

$$\nu\{3/2^-[512]9/2^+[624]11/2^+[615]\},$$

$$E_x^{\rm cal}+E^{\rm GM}=1937-150=1787\ \text{keV}.$$

The predicted $(g_K^{\rm cal}-g_R)$ values agree with the measured ones at the lower spin states (see Table II). The two-quasineutron $\nu 10^+\{9/2^+[624]11/2^+[615]\}$ states are also known at low excitation energies in the neighboring even-even nuclei ^{184}Os [2], ^{186}Os [19] and ^{182}W [35]. Furthermore, the $\nu\{3/2^-[512]9/2^+[624]11/2^+[615]\}$ state is observed at 2050 keV in ^{183}W [36]. We therefore assign this configuration to band IV.

4. The K=(41/2) isomer at 5007 keV

Since the $E_x=5007$ keV state has the half-life of 18 ns, it can be considered as an intrinsic state having $K=41/2$ rather than an excited state in a rotational band. Following configurations give rise to low-lying $K=41/2$ states in ^{185}Os:

$$K^\pi=41/2^-,\nu\{1/2^-[510]1/2^-[521]7/2^-[503]\times 9/2^+[624]11/2^+[615]\}\otimes\pi\{5/2^+[402]7/2^+[404]\},$$

$$E_x^{\rm cal}+E^{\rm GM}=5182+28=5210\ \text{keV},$$

$$K^\pi=41/2^+,\nu\{1/2^-[510]1/2^-[521]3/2^-[512]\times 9/2^+[624]11/2^+[615]\}\otimes\pi\{7/2^+[404]9/2^-[514]\},$$

$$E_x^{\rm cal}+E^{\rm GM}=5640-401=5239\ \text{keV},$$

$$K^\pi=41/2^-,\nu\{1/2^-[521]3/2^-[512]7/2^-[503]\times 9/2^+[624]11/2^+[615]\}\otimes\pi\{1/2^-[541]9/2^-[514]\},$$

$$E_x^{\rm cal}+E^{\rm GM}=5712-365=5347\ \text{keV}.$$

Due to the lack of information such as alignments or g_K factors, the configuration assignment is not conclusive.

TABLE IV. Hindrance factors for the K-forbidden transitions from multiquasiparticle states in ^{185}Os.

K_i^π	E_γ (keV)	$T_{1/2}^\gamma$ (ns)	ΔK	$L\lambda$	F	f_ν
$19/2^+$	268.7	$\leqq 53$		$M1$	$\leqq 4.6\times10^4$	
	566.8	$\leqq 28$	4	$M1$	$\leqq 2.3\times10^5$	$\leqq 61$
	814.9	$\leqq 9$	4	$M1$	$\leqq 2.2\times10^5$	$\leqq 60$
	1001.1	$\leqq 38$	4	$E2$	$\leqq 4.3\times10^3$	$\leqq 66$
$23/2^-$	142.7	55	2	$E1$	7.5×10^5	7.5×10^5
	231.2	7.7	10	$E2$	0.57	0.83
	633.5	255	11	$E2$	2.9×10^3	2.4
$27/2^-$	(52)			$M1$		
	337.8	$\leqq 13$	2	$M1$	$\leqq 2.2\times10^4$	$\leqq 2.2\times10^4$
	405.0	$\leqq 40$	2	$E2$	$\leqq 49$	
	615.1	$\leqq 13$	2	$E2$	$\leqq 1.3\times10^2$	
$(31/2^-)$	326.7	$\leqq 26$	1	$M1$	$\leqq 4.1\times10^4$	
	653.9	$\leqq 6.5$	15	$E2$	$\leqq 87$	$\leqq 1.4$

D. Hindrances of transitions

Transitions which involve K changes larger than the transition multiple order, i.e., $\Delta K>\lambda$, are forbidden in the K selection rule. Such transitions are therefore called K-forbidden transitions. The hindrance of K--forbidden transitions can be discussed in terms of hindrance factors F or hindrance factors per degree of K forbiddenness f_ν defined as

$$f_\nu=F^{1/\nu}=(T_{1/2}^\gamma/T_{\rm W})^{1/\nu}, \tag{5}$$

where ν is the order of K forbiddenness, $T_{1/2}^\gamma$ and $T_{\rm W}$ are, respectively, the partial γ-ray half-life and the corresponding Weisskopf single-particle estimate. Several K-forbidden transitions have been observed in ^{185}Os. Table IV summarizes the γ-ray branchings from multiquasiparticle states and the hindrance factors. Since the $K^\pi=19/2^+$, $27/2^-$, and $31/2^-$ levels have no measurable half-lives, the upper limit of the present detection system, $T_{1/2}\leqq 5$ ns, is used.

The hindrance factors for transitions from the $K^\pi=19/2^+$ and $27/2^-$ states are within the range of the systematic values [37,38]. On the other hand, the 231 and 634 keV transitions from the $K^\pi=23/2^-$ state, and the 654 keV transition from the $K^\pi=31/2^-$ state exhibit low hindrances despite the large K inhibition. The low hindrance of the 231 keV transition $(F=0.57)$ can be explained as follows. The $I^\pi=19/2^-$ 1756 keV state in the $3/2^-[512]$ populated by the 231 keV transition has a fragmented decay into several states including the $I^\pi=19/2^+$ high-K state in the band III $(K^\pi=19/2^+)$. This could indicate that the 1756 keV state has high-K components which would in part explain the low hindrance of the 231 keV transition.

For the 634 and 654 keV transitions with $\Delta K=11$ and 15, respectively, hindrance factors of $F=2.9\times10^3$ and $F\leqq 87$ have been obtained. Similar transitions with large ΔK values and low hindrances $(f_\nu=2.3$–5.5 with $\Delta K=14$ and 16) have been observed in ^{182}Os [2], ^{174}Hf [3], and ^{176}W [4]. So far, two different K-mixing mechanisms involving shape fluctuation with respect to γ deformation [2,4,8,9] and Fermi-

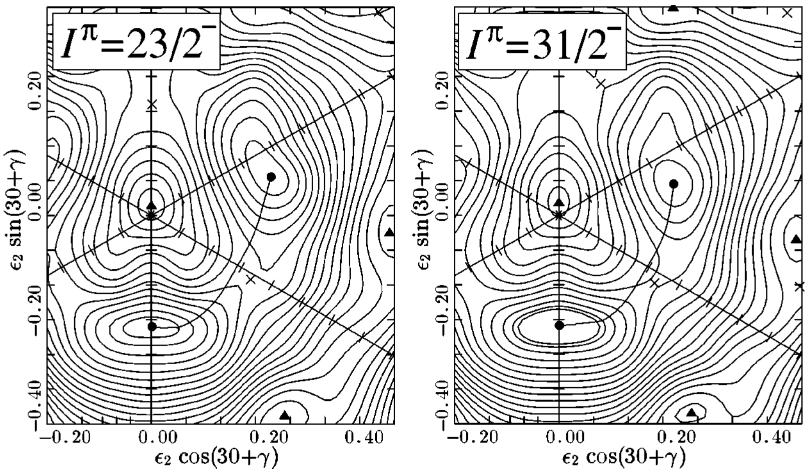

FIG. 9. The potential energy surface for the $I^\pi=23/2^-$ and $31/2^-$ states in ^{185}Os. The potential minima and maxima are marked by solid circles and solid triangles, while the saddle points are marked by crosses. The solid curves show the least action paths which go on a slanting surface. The energy contour is drawn at intervals of 500 keV.

alignment Coriolis interaction [3,5–7] have been proposed. For the large $\Delta K(\geqq 10)$ transitions, the importance of the γ degree of freedom is emphasized by calculation using a γ tunneling model [9,20,39]. In the following, the decay rates for the $I^\pi=23/2^-$ and $31/2^-$ states will be discussed within the framework of the γ tunneling model.

In the γ tunneling model [9], no direct mixing between low-K and high-K states is assumed. The low-K (high-K) wave function can penetrate to the high-K (low-K) state by tunneling through a potential barrier along the γ-deformation path. The tunneling probability is defined in the semiclassical tunneling approximation as

$$T = \left[1 + \exp\left(\frac{2W}{\hbar}\right)\right]^{-1}, \tag{6}$$

where W is the WKB action, $\int\sqrt{2M_0(V-E_0)}ds$. Here, V is the potential energy along the least action path s, and E_0 is the zero-point energy of the high-K (initial) state. The least action can be calculated by evaluating the mass parameter M_0 and the potential energy V at a given angular momentum [9]. The mass parameter depends on the effective pairing gap $\Delta_{\rm eff}$ in the random phase approximation method [40], proportional to $\Delta_{\rm eff}^{-2}$ [41], and thus increases along with a spin caused by a smaller pairing gap. The potential barrier also changes with variation in spin, i.e., the barrier height decreases as the nuclear shape becomes softer with respect to γ deformation. The tunneling probabilities therefore depend on these two effects. For heavier Os nuclei, the least actions decrease with increasing spins due to the softness towards triaxiality [20]. As shown in Fig. 9, the potential energy surface at $I^\pi=31/2^-$ in ^{185}Os becomes more triaxial than at $I^\pi=23/2^-$, resulting in a smaller least action for $I^\pi=31/2^-$ (see Table V).

Assuming that the tunneling process is independent of the electromagnetic process, the tunneling transition probability can be obtained as a product of the in-band transition rate and the squared mixing amplitude $\alpha^2 \approx (E_0/\pi\Delta E)^2 T$ where ΔE is the observed energy difference of the coupling states [9]. For stretched $E2(\Delta I=2)$ transitions, the reduced transition probability thus becomes

$$B(E2)^{\rm cal} = \alpha(I)^2 \frac{5}{16\pi} Q_0^2 \langle IK20|I-2K\rangle^2, \tag{7}$$

where the quadrupole moment Q_0 and the K value are those for the final state. The calculated hindrance is then written as $B(E2)^{\rm W}/B(E2)^{\rm cal}$ using the Weisskopf estimate of the reduced transition probability, $B(E2)^{\rm W}$. Table V summarizes the calculated results for the 634 and 654 keV $E2$ transitions in ^{185}Os. The calculated low hindrances are due to the small least actions as well as the small energy difference of $\Delta E=58$ keV at $I^\pi=23/2^-$ and $\Delta E=12$ keV at $I^\pi=31/2^-$, and are consistent with the observed hindrances within two orders of magnitude. Here we note that the observed energy difference rather than the calculated value is used for ΔE since the standard Struntinsky-typed potential energy surface calculation used in the present γ-tunneling model does not properly reproduce the energy difference without, e.g., alternating the single-particle energies. The calculated energy levels deviates from the observed ones by 500–1000 keV in the present case (see Fig. 9). Nevertheless, the calculated tunneling probabilities are robust because they are mainly determined by the height of potential barrier which is far from the potential minima.

The present data together with those available for the large $\Delta K(\geqq 10)$ transitions in Hf,W, and Os nuclei (see Fig. 16 in Ref. [20]) show a clear correlation between the measured and calculated hindrances. It can be concluded that the γ tunneling is an important process to introduce the large ΔK mixing between the low-K and high-K states. In our recent work [42], we have shown that the action values of the Os nuclei are considerably smaller than those of, e.g., Hf,W

TABLE V. Comparison of the calculated and measured hindrance factors for the $E2$ transitions from the $K^\pi=23/2^-$ and $(31/2^-)$ states in ^{185}Os.

K_i^π	E_γ (keV)	ΔK	W ($\hbar$)	E_0 (MeV)	Q_0 (e b)	$F_{\rm cal}$	$F_{\rm exp}$
$23/2^-$	634	11	6.55	0.555	6.8	2.1×10^2	2.9×10^3
$(31/2^-)$	654	15	5.00	0.507	6.5	0.52	<87

nuclei. This trend correlates well with the excitation energy of the γ vibrational $I^{\pi}=2^{+}$ states which is known as an indicator of γ softness (see Figs. 5 and 6 in Ref. [42]), although the mechanisms of the two underlying collective motions, the small amplitude vibrations and the large amplitude tunneling, are different.

It should be noted, however, that the difference between the calculated and measured hindrance factors becomes large for the heavier Os nuclei ($N \geqq 107$) where the lower hindrances are observed. In addition, the calculated hindrance factors are smaller than the experimental values, i.e., the calculated transition strength is larger than the observed one which indicates difficulties with the present γ-tunneling model. This would indicate that the calculated potential surface is too flat. In the case of small actions, the height of the potential barrier in the tunneling process is low, so that the calculated actions sensitively vary with the parameters such as the Nilsson potential, the tunneling mass parameter, and the zero-point energy which are involved in the γ tunneling calculations. The observed discrepancy would be reduced by optimizing such parameters, which is, however, beyond the scope of the present work. From this point of view, further studies on high-K isomeric decays in the heavier Os nuclei would give an opportunity for more detailed investigation of the γ-tunneling process.

The $I=(41/2)$ isomer at 5007 keV has been identified to have $T_{1/2}=18(2)$ns. It decays to the $I=(39/2)$ state via a 426 keV K-allowed transition which has dipole character. The hindrance factor is calculated to be $F=6.2\times10^{4}$ assuming $M1$, or $F=6.5\times10^{6}$ assuming $E1$. These are within the systematic values [38] for K-allowed $M1(F=1-10^{4})$ and $E1(F=10^{3}-10^{7})$ transitions. In order to discuss this in more detail, further experimental information on the multipolarity is necessary.

V. SUMMARY

High-spin states in ^{185}Os have been studied using the ^{176}Yb(^{13}C,4n) reaction. Four new rotational bands based on the γ-vibrational, and the three-quasiparticle excitations have been observed. From the comparison of the measured g_K factors and excitation energies with the theoretical values, Nilsson configurations were assigned. A $K=(41/2)$ isomer at 5007 keV has been identified with a half-life of $T_{1/2}=18(2)$ ns. The large ΔK transitions observed in ^{185}Os have been analyzed in terms of the γ tunneling model. The result confirms our previous conclusion that K mixing due to γ softness is important for large ΔK transitions. More detailed investigation on the γ-tunneling model is required to remove the observed discrepancy between the measured and calculated hindrance factors for the heavier Os nuclei.

ACKNOWLEDGMENTS

The tandem accelerator at the Niels Bohr Institute was shut down at the end of 1998, but we still owe the staff many thanks for their skillful operation. This work was supported by the Danish Natural Science Research Council.

[1] P. M. Walker and G. D. Dracoulis, Nature (London) **399**, 35 (1999).
[2] P. Chowdhury, B. Fabricius, C. Christensen, F. Azgui, S. Bjørnholm, J. Borggreen, A. Holm, J. Pedersen, G. Sletten, M. A. Bentley, D. Howe, A. R. Mokhtar, J. D. Morrison, J. F. Sharpey-Schafer, P. M Walker, and R. M. Lieder, Nucl. Phys. **A485**, 136 (1988).
[3] P. M. Walker, G. Sletten, N. L. Gjørup, M. A. Bentley, J. Borggreen, B. Fabricius, A. Holm, D. Howe, J. Pedersen, J. W. Roberts, and J. F. Sharpey-Schafer, Phys. Rev. Lett. **65**, 416 (1990); N. L. Gjørup, P. M. Walker, G. Sletten, M. A. Bentley, B. Fabricius, and J. F. Sharpey-Schafer, Nucl. Phys. **A582**, 369 (1995).
[4] B. Crowell, P. Chowdhury, S. J. Freeman, C. J. Lister, M. P. Carpenter, R. G. Henry, R. V. F. Janssens, T. L. Khoo, T. Lauritsen, Y. Liang, F. Soramel, and I. G. Bearden, Phys. Rev. Lett. **72**, 1164 (1994); B. Crowell, P. Chowdhury, D. J. Blumenthal, S. J. Freeman, C. J. Lister, M. P. Carpenter, R. G. Henry, R. V. F. Janssens, T. L. Khoo, T. Lauritsen, Y. Liang, F. Soramel, and I. G. Bearden, Phys. Rev. C **53**, 1173 (1996).
[5] P. M. Walker, G. D. Dracoulis, A. P. Byrne, B. Fabricius, T. Kibèdi, and A. E. Stuchbery, Phys. Rev. Lett. **67**, 433 (1991).
[6] P. M. Walker, K. C. Yeung, G. D. Dracoulis, P. H. Regan, G. J. Lane, P. M. Davidson, and A. E. Stuchbery, Phys. Lett. B **309**, 17 (1993).
[7] S. Frauendorf, in *Proceedings of the International Conference on The Future of Nuclear Spectroscopy, Crete, 1993*, edited by W. Gelletly, C. A. Kalfas, R. Vlastou, S. Harissopulos, and D. Loukas (National Center for Scientific Research, Demokritos, Athens, 1994), pp. 112–127.
[8] T. Bengtsson, R. A. Broglia, E. Vigezzi, F. Barranco, F. Dønau, and Jing-ye Zhang, Phys. Rev. Lett. **62**, 2448 (1989).
[9] K. Narimatsu, Y. R. Shimizu, and T. Shizuma, Nucl. Phys. **A601**, 69 (1996).
[10] D. C. Radford, Nucl. Instrum. Methods Phys. Res. A **361**, 297 (1995).
[11] K. S. Krane, R. M. Steffen, and R. M. Wheeler, Nucl. Data Tables **11**, 351 (1973).
[12] L. P. Ekström and A. Nordlund, Nucl. Instrum. Methods Phys. Res. A **313**, 421 (1992).
[13] B. Harmatz, T. H. Handley, and J. W. Mihelich, Phys. Rev. **128**, 1186 (1962).
[14] H. L. Sharma and N. M. Hintz, Phys. Rev. C **13**, 2288 (1976).
[15] H. Sodan, W. D. Fromm, L. Funke, K. H. Kaun, P. Kemnitz, E. Will, G. Winter, and Y. Berzin, Nucl. Phys. **A237**, 333 (1975).
[16] D. Balabanski, W. Gast, G. Hebbinghaus, R. Lieder, T. Rzaca-Urban, H. Schnare, and W. Urban, C. R. Acad. Bulg. Sci. **49**, 25 (1996); D. L. Balabanski, W. Gast, G. Hebbinghaus, A. Krämer-Flecken, R. M. Lieder, T. Rzaca-Urban, H. Schnare, and W. Urban, JUL-Spez-499 (1989), pp. 46.
[17] R. S. Hager and E. C. Seltzer, Nucl. Data, Sect. A **4**, 1 (1968).
[18] R. Bengtsson and S. Frauendorf, Nucl. Phys. **A327**, 139

(1979).
[19] C. Wheldon, P. M. Walker, P. H. Regan, T. Saitoh, N. Hashimoto, G. Sletten, and F. R. Xu, Phys. Rev. C **59**, R2334 (1999); Nucl. Phys. **A652**, 103 (1999).
[20] T. Shizuma, K. Matsuubara, Y. Toh, Y. Hayakawa, M. Oshima, Y. Hatsukawa, M. Matsuda, K. Furuno, Y. Sasaki, and T. Komatsubara, Nucl. Phys. **A696**, 337 (2001).
[21] T. Shizuma, S. Mitarai, G. Sletten, R. A. Bark, N. L. Gjørup, H. J. Jensen, J. Wrzesinski, and M. Piiparinen, Nucl. Phys. **A593**, 247 (1995).
[22] A. Neskakis, R. M. Lieder, M. Müller-Veggian, H. Beuscher, W. F. Davidson, and C. Mayer-Böricke, Nucl. Phys. **A261**, 189 (1976).
[23] P. M. Walker, G. D. Dracoulis, A. P. Byrne, B. Fabricius, T. Kibèdi, A. E. Stuchbery, and N. Rowley, Nucl. Phys. **A568**, 397 (1994).
[24] A. Bohr and B. R. Mottelson, *Nuclear Structure* (Benjamin, Reading, 1975), Vol. 2.
[25] R. A. Bark, G. B. Hagemann, B. Herskind, H .J. Jensen, W. Korten, J. Wrzesinski, H. Carlsson, M. Bergström, A. Brockstedt, A. Nordlund, H. Ryde, P. Bosetti, S. Leoni, F. Ingebretsen, and P. O. Tjøm, Nucl. Phys. **A591**, 265 (1995).
[26] F. Dönau and S. Frauendorf, in *High Angular Momentum Properties of Nuclei*, edited by N. R. Johnson (Harward Academic, Chur, Switzerland, 1983), p. 143; F. Dönau, Nucl. Phys. **A471**, 469 (1987).
[27] H. Morinaga and T. Yamazaki, *In-Beam Gamma-Ray Spectroscopy* (North-Holland, Amsterdam, 1975).
[28] A. K. Jain, R. K. Sheline, P. C. Sood, and Iran Jain, Rev. Mod. Phys. **62**, 393 (1990).
[29] G. Audi and A. H. Wapstra, Nucl. Phys. **A595**, 409 (1995).
[30] C. J. Gallagher and S. A. Moszkowski, Phys. Rev. **111**, 1282 (1958).
[31] K. Jain, O. Burglin, G. D. Dracoulis, B. Fabricius, N. Rowley, and P. M. Walker, Nucl. Phys. **A591**, 61 (1995).
[32] C. Fahlander and G. D. Dracoulis, Nucl. Phys. **A375**, 263 (1982).
[33] R. M. Lieder, G. Sletten, J. Borggreen, and J. Pedersen, Nucl. Phys. **A375**, 291 (1982).
[34] R. B. Firestone, *Table of Isotopes*, 8th ed. (Wiley-Interscience, New York, 1996).
[35] B. D. Jeltema, F. M. Bernthal, T. L. Khoo, and C. L. Dors, Nucl. Phys. **A280**, 93 (1977).
[36] T. R. Saitoh, N. Saitoh-Hashimoto, G. Sletten, R. A. Bark, M. Bergström, P. Regan, S. Tömaänen, P. G. Varmette, P. M. Walker, and C. Wheldon, Nucl. Phys. **A669**, 381 (2000).
[37] P. M. Walker, J. Phys. G **16**, L233 (1990).
[38] K. E. G. Løbner, Phys. Lett. **26B**, 369 (1968).
[39] T. Shizuma, G. Sletten, R. A. Bark, I. G. Bearden, S. Leoni, M. Mattiuzzi, S. Mitarai, S. W. O degaard, S. Skoda, K. Sträle, J. Wrzesinski, and Y. R. Shimizu, Nucl. Phys. **A626**, 760 (1997).
[40] Y. R. Shimizu and R. A. Broglia, Nucl. Phys. **A515**, 38 (1990).
[41] F. Barranco, G. F. Bertsch, R. A. Broglia, and E. Vigezzi, Nucl. Phys. **A512**, 253 (1990).
[42] Toshiyuki Shizuma, Yoshifumi R. Shimizu, and Takehito Hayakawa, J. Nucl. Sci. Technol. **39**, 1137 (2002).